

Key Points:

- Seasonal variability of the BC is out-of-phase with the Sverdrup transport due to baroclinic adjustment
- The BC transport variability is associated to the wind stress curl in the western part of the basin and coastal upwelling
- In the 2009/2010 event, anticyclonic winds lower the coastal sea level, and warm anomalies increase sea level offshore, strengthening the BC

Supporting Information:

- Supporting Information S1
- Figure S1
- Figure S2

Correspondence to:

M. Goes,
marlos.goes@noaa.gov

Citation:

Goes, M., Cirano, M., Mata, M. M., & Majumder, S. (2019). Long-term monitoring of the Brazil Current transport at 22°S from XBT and altimetry data: Seasonal, interannual, and extreme variability. *Journal of Geophysical Research: Oceans*, 124. <https://doi.org/10.1029/2018JC014809>

Received 26 NOV 2018





Accepted 23 APR 2019

Accepted article online 6 MAY 2019

©2019. The Authors.

This is an open access article under the terms of the Creative Commons Attribution-NonCommercial-NoDerivs License, which permits use and distribution in any medium, provided the original work is properly cited, the use is non-commercial and no modifications or adaptations are made.

Long-Term Monitoring of the Brazil Current Transport at 22°S From XBT and Altimetry Data: Seasonal, Interannual, and Extreme Variability

M. Goes^{1,2} , M. Cirano³ , M. M. Mata⁴ , and S. Majumder^{1,2,5} 

¹Cooperative Institute for Marine and Atmospheric Studies (CIMAS), University of Miami, Miami, FL, USA, ²Atlantic Oceanographic and Meteorological Laboratory, National Oceanic and Atmospheric Administration, Miami, FL, USA,

³Department of Meteorology, Institute of Geosciences, Federal University of Rio de Janeiro (UFRJ), Rio de Janeiro, Brazil,

⁴Institute of Oceanography, Federal University of Rio Grande (FURG), Rio Grande, Brazil, ⁵Now at Department of Marine Sciences, University of Georgia, Athens, GA, USA

Abstract The seasonal and interannual variability of the Brazil Current (BC) at 22°S is examined using expendable bathythermograph (XBT) transect and satellite altimetry data from 1993 to 2017. The XBT-based mean absolute geostrophic transport of the BC is estimated as 4.7 ± 1.9 Sv, with additional 0.9 ± 0.9 Sv along the shelf. The strong agreement between the absolute dynamic height and altimetric sea surface height is used in two methods to reconstruct a daily time series of the BC transport since 1993. The altimetry-based methods can represent well the BC transport seasonal cycle, whereas the XBT-based estimates are slightly aliased by the strong regional mesoscale variability. At interannual timescales, the BC transport is significantly correlated ($r = 0.43$) with the wind stress curl in the western half of the basin with a lag of 19 months, which is consistent with baroclinic adjustment timescales. Other sources of variability can be observed in a case study of the summer 2009/2010 event, which was characterized by strong sea surface temperature anomalies of approximately 3 °C. During the event, the BC reached 11 Sv for nearly 3 months, partly driven by an increased coastal upwelling from a cyclonic wind stress anomaly, a standing eddy along the section, and thermocline anomalies that reached the offshore side of section in February. Heat anomalies were transported southward along the subtropical gyre following the BC path in a period of 2 months, which is consistent with advective timescales. Potential implications for extreme sea level and summer precipitation events in South America are discussed.

Plain Language Summary Two methods were developed to create a 25-yearlong time series of the Brazil Current (BC) volume transport across 22°S using expendable bathythermograph data and altimetry. The seasonal variability of the BC is out-of-phase with the wind stress curl across the basin, suggesting that wave adjustment and local winds control the seasonality. At interannual timescales, the wind stress curl in the western side of the basin and the regional upwelling control the BC variability. In the summer of 2009/2010, the BC transport was 3 times stronger than its mean. The event was characterized by a strong warm sea surface temperature anomaly propagating westward into the region and an associated anticyclonic wind stress anomaly. Results suggest that the BC strengthening was linked to a decreased near-shore sea level of ~20 cm due to increased coastal upwelling, and an increased offshore sea level of 15 cm influenced by the warm anomaly.

1. Introduction

The Brazil Current (BC) is the Western Boundary Current that closes the South Atlantic subtropical gyre. The formation of the BC occurs between 10°S and 15°S (Figure 1a) from the southern branch of the South Equatorial Current bifurcation (e.g., Peterson & Stramma, 1991; Rodrigues et al., 2007). The BC flows southward from its formation region as a weak surface current, intensifying along its path by central and intermediate water contributions. At approximately 38°S, the BC encounters the Malvinas Current, forming one of the most energetic regions in the world's ocean (Garzoli and Garrafo, 1989; Goni et al., 1996; Piola et al., 2008). Near Cabo Frio (~23°S, 42°W), the BC is characterized by intense meandering and occasional eddy shedding (da Silveira et al., 2008; Pilo et al., 2015), and these features of the BC dynamics have been associated to modulations in coastal upwelling (e.g., Calado et al., 2006; Campos et al., 2000). The Cabo Frio upwelling, which is stronger during the austral summer, creates a strong sea surface temperature (SST) front by bringing cold

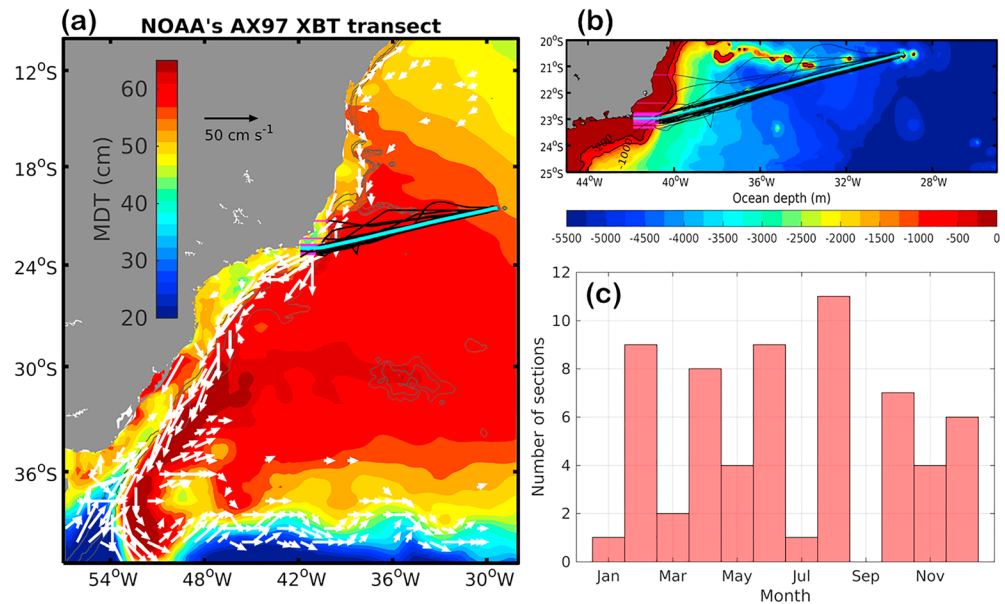


Figure 1. (a) Map of mean dynamic topography (MDT) overlaid by the mean climatological surface velocity vectors derived from drifter data (Laurindo et al., 2017) with a cutoff of 7 cm/s and the location of the 62 sections from the AX97 high-density XBT transect used in this study (black lines). Magenta lines are the extrapolations applied to the XBT sections onto the shelf, and light blue line is the location of the mean transect used in the Brazil Current reconstruction from satellite altimetry. (b) Zoom over the AX97 region showing the AX97 sections of (a) overlaid on the contours of the local bathymetry (m). (c) Histogram with the monthly distribution of the 62 realizations of the AX97 transect.

central waters to the surface, enhancing the local biological productivity (Gonzalez-Rodriguez et al., 1992), decreasing the coastal sea level via Ekman divergence, and forcing the marine boundary layer and surface turbulent fluxes, with potential impact on the weather patterns in the Southeast South America (e.g., Chelton et al., 2007; Pezzi et al., 2016; Ribeiro et al., 2011). Evans and Signorini (1985) described the BC near 23°S as a 400- to 500-m-deep surface boundary current with a southward volume transport offshore of the shelf break of approximately 6 Sv (1 Sv = 10^6 m³/s). In a recent paper, Schmid and Majumder (2018) summarized the previous literature of BC transport between 19°S and 22.5°S ranging from 1 to 7 Sv.

The variability of the BC can be at least partially determined by the Sverdrup balance, in which the large-scale distribution of wind stress curl (WSC) determines the gyre patterns of ocean circulation. The relatively low magnitude of the BC transport compared to its North Atlantic counterpart, the Gulf Stream, is a result of the compensating influence of the wind-driven and thermohaline components of the general circulation (Stommel, 1965, p. 170). The variability of the BC modulates the thermohaline circulation and distribution of heat across the South Atlantic (Dong et al., 2014), and the convergence of heat in the South Atlantic can potentially lead to local and global climate impacts (Lopez et al., 2016).

Climate models predict a strengthening of several global Western Boundary Current systems as consequence of an increase of WSC within the subtropical gyres (Pontes et al., 2016; Wu et al., 2012), in addition to a poleward expansion of the tropical and subtropical regions due to global warming (Goni et al., 2011; Waugh et al., 2015). Challenges to understand long-term variability of boundary currents come from the scarcity of observations across the boundaries, regions that often present variability stronger than their mean value (Vianna & Menezes, 2011). The physical processes affecting boundary currents are not generally coherent across different latitudes, which can include from interaction of the flow with bottom topography, thermohaline circulation, and recirculation components (Deser et al., 1999; Wunsch & Roemmich, 1985).

Previous studies on the BC focused primarily on its unique mesoscale variability using for this regional ocean models and short-term synoptic hydrographic surveys (e.g., Bilo et al., 2014; Rocha et al., 2014). Recent efforts to understand the interannual-to-decadal variability of the BC are mostly focused near the Brazil-Malvinas Confluence or using numerical models (Artana et al., 2018; Assad et al., 2015; Combes & Matano, 2014). However, little is still known about the interannual variability of the BC

north of the Confluence, particularly from observations, and its link to regional sea level and large-scale processes of heat and momentum advection. Within the last two decades, the inclusion of repeat high-density expendable bathythermograph (XBT) transects across the BC in two latitudes (AX97 at 22°S and AX18 at 34.5°S) has provided the longest continuous observational system in place to monitor the variability of the BC. The objective of this paper is to examine the seasonal and interannual variability of the BC and to quantify the main drivers of this variability. For this, we introduce two methodologies to estimate the absolute geostrophic velocity of the BC across 22°S and use them to produce daily, long-term time series of the BC volume transport. This latitude is important because it is close to the Cabo Frio upwelling system and is the region where the South Atlantic Convergence Zone summertime rain belt has a strong oceanic signature (Carvalho et al., 2004). Moreover, the region lies close to the Vitoria-Trindade submarine ridge (Figure 1b), a feature that exerts a strong influence in the South Atlantic intermediate circulation via eddy-topography interaction (Costa et al., 2017; Schmid et al., 1995). This paper is structured as follows: in section 2, we introduce the main data sets used and the methodologies to reconstruct the BC velocity and derived volume transport using altimetry; section 3 examines the temporal variability of the BC and its impact on the unusually warm summer of 2009-2010 event in the western South Atlantic; section 4 concludes this study and provides recommendations for future work.

2. Data and Methods

2.1. Data

In this study, we focus on the variability of the BC across 22°S. To estimate relevant parameters of the BC variability at 22°S, we use 62 realizations of the AX97 repeat high-density XBT transect for the period spanning from 2004 to 2017. The AX97 samples the upper ocean temperature from Rio de Janeiro to Trindade Island approximately five times a year, which allows at least 10 transects per season, therefore producing little seasonal sampling bias (Figure 1c). Each transect has an average spacing between samplings of approximately 27 km, with increasing resolution to 18 km near the coast and near Trindade Island. Salinity is estimated using historical T-S relationships for the region, according to the method of Goes et al. (2018). The temperature and salinity fields of each transect realization are interpolated along track onto a regular 0.2° longitudinal spacing (approximately 25 km) using a Lowess filtering with half-power points of 2° and 0.8°.

Gridded multimission altimetric sea surface height (SSH) data used in this study are from the delayed time, daily Ssalto/Duacs product, produced by the Archiving, Validation and Interpretation of Satellite Oceanographic data and distributed by the Copernicus Marine and Environment Monitoring Service (www.marine.copernicus.eu). Among others, corrections for ocean tides (Carrere et al., 2016) and barometric pressure effects (Carrere, & Lyard, 2003) are applied to the SSH data. A subset is analyzed from the South Atlantic domain for the period from January 1993 to December 2017 and available at a horizontal grid resolution of $1/4^\circ \times 1/4^\circ$. Sea surface height anomalies (SSHA) are computed relative to 1993–2012 period mean. Satellite SST data used are from the Optimum Interpolation Sea Surface Temperature daily product (Reynolds et al., 2007) at a $1/4^\circ$ spatial resolution from 1993 to 2017. Monthly wind stress fields are obtained from the ERA-Interim data assimilation product (Dee et al., 2011) gridded at a 0.75° resolution also from 1993 to 2017.

2.2. Methods

In this section, we describe the methodology to infer the absolute geostrophic velocities and volume transport of the BC using altimetry and hydrographic data.

2.2.1. Geostrophic Velocities

The relative dynamic height is calculated from the temperature and salinity profiles, assuming a reference level at $z = 500$ m, which is approximately the interface between the Central and Intermediate waters near the $\sigma_\theta = 26.8\text{-kg/m}^3$ isopycnal surface (Biló et al., 2014; da Silveira et al., 2008; Lima et al., 2016). The absolute dynamic height (DH(z)) is calculated by imposing at the reference depth the respective monthly climatology value of absolute dynamic topography (ADT). The climatological ADT values are from the International Pacific Research Center gridded merged altimetry and Argo product (e.g., Yu

et al., 2006). Absolute geostrophic velocities across the section are derived from $DH(z)$ using the thermal wind relationship.

2.2.2. Extrapolation to the Shelf

Using ocean reanalysis data, Lima et al. (2016) estimated that approximately 30% of the BC flows along the shelf across 22.5°S. The shelf contribution is often not captured by the AX97 transect, because several of its realizations end/start offshore of the 200-m isobath. Therefore, an extrapolation method can be used as a resort to overcome this operational issue. Tools for extrapolating a hydrographic section to the shelf have long been proposed. For instance, this could be achieved by extending the closest horizontal gradients of temperature and dynamic height onto the shelf (Montgomery, 1941; Reid & Mantyla, 1976). Given the importance of the shelf contribution to the BC transport, we developed a method to use satellite altimetry data to extrapolate the AX97 dynamic height data toward the shelf. With this aim, the first step is to interpolate altimetric SSH data to the same day and location of each XBT profile. Next, from the XBT profile location closest to the shore, SSH data are resampled westward at 0.2° intervals of longitude. Then, the XBT-derived surface absolute dynamic heights ($DH_i(z=0)$), where the subscript i indicates the longitudinal location and increases offshore, are extrapolated toward the shelf using the local gradients of SSH. Mathematically, the equation to derive the extrapolation to the next location closer to the shelf ($i-1$) from the $DH_i(z)$ data at the longitudinal location (i) and depth (z) is the following:

$$DH_{i-1}(z) = DH_i(z) - \frac{(SSH(i) - SSH(i-1))}{pa(z)} \quad (1)$$

In equation (1), $pa(z) = 1/\exp(z/300)$; thus, the surface dynamic height information is extrapolated in depth using an exponential decay with an e -folding depth scale of 300 m, which was chosen from several sensitivity tests in that particular region, and agrees with previously estimated decay of eddy variance of dynamic height near the boundary (e.g., Hautala et al., 1994). Additional extrapolation of DH below 300 m onto the boundary is performed at each depth using a seventh-order autoregressive method. The application of this methodology is possible because there is generally a good agreement between SSH and the surface DH referenced to the International Pacific Research Center ADT climatology at 500 m in all sections (Figure 2, upper panels). This method generates smooth transitions between the shelf and interior velocities (Figure 2), and the original velocities remain practically unchanged.

2.2.3. Transport Calculations

The absolute geostrophic BC transport estimated for the AX97 XBT data (T_{AX97}) is calculated by integrating the cross-section velocities in the top 500 m from 41°W and the location of the minimum cumulative transport between 41°W and 36°W. After the eastern limit of the BC is found, the transport is calculated between these two locations taking into account only the southward velocities, which represent the BC flow. To extend the BC transport across 22.5°S in time from January 1993 to December 2017, two methods are used applying daily SSH maps along a reference transect estimated as the average location of all considered transects (Figure 1). In addition, the BC transport will be compared to the integrated Sverdrup transport and the upwelling near 22.5°S. These methods are defined as follows.

- i Synthetic method (*SYNTH*). Here we use the methodology described in Goes et al. (2013) to estimate synthetic transports of the BC. For this, $DH(0)$ is regressed onto the $DH(z)$ values at each depth and longitude. Correlation values between the regressed $DH(0)$ and $DH(z)$ are typically above 0.9 in the whole depth of the section. $DH(0)$ is then regressed to SSH, with both fields detrended and demeaned, establishing the link between altimetric and hydrographic quantities. The agreement between $DH(0)$ and SSH is very good along the AX97 section (Figure 3), with local differences typically below 3 cm and an overall $R^2 = 0.71$ for the regression between these two quantities. Geostrophic velocities are then estimated from the synthetic DH using the thermal wind relationship, and transport is calculated from the velocity fields similarly to the AX97 data. The BC core velocities estimated using this method show strong agreement with the ones estimated with XBTs (Figure 4a).
- ii SSH gradient method (ΔSSH). This method uses the SSH gradients to estimate the BC transport. Previous studies have used similar methodology to calculate the transport of other Western Boundary Currents (Imawaki et al., 2001; Park & Sweet, 2015; Wunsch et al., 1969). Using a one 1/2 layer geostrophic approximation, we calculated the transport according to the following equation:

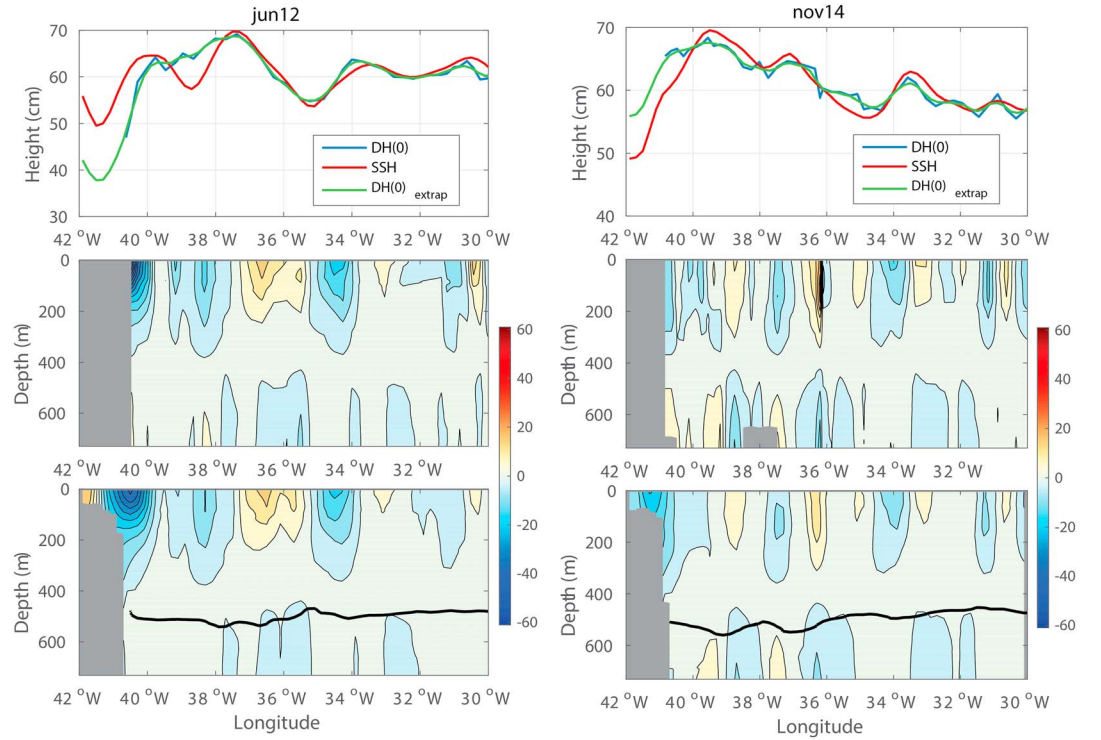


Figure 2. Example for June 2012 and November 2014 of the method to extend the dynamic height estimates (DH) to the shelf. (upper panels) Comparison between the surface DH (cm) derived from XBT observations, sea surface height (SSH) from altimetry, and the extrapolated DH used to calculate the Brazil Current properties. (middle panels) Absolute geostrophic velocity (cm/s) derived from the original DH data. (lower panels) Absolute geostrophic velocity (cm/s) derived from the extrapolated DH. Thick black line in the lower panels is the depth of the $\sigma_{\theta} = 26.8 \text{ kg/m}^3$. DH = dynamic height.

$$T_{\Delta\text{SSH}} = \frac{g}{f} \int_0^h \int_{x_1}^{x_2} \frac{d\text{SSH}}{dx} dx dz = \frac{gh}{f} \Delta\text{SSH} \quad (2)$$

where g is gravity, f is the Coriolis parameter, h is the layer depth, and ΔSSH is the SSH difference along the AX97 transect between x_1 and x_2 , the western boundary, and the location of the maximum SSH value, respectively. To integrate T_{SSH} considering only southward velocities, only the $d\text{SSH} > 0$ values are maintained in equation (2). The parameter value $h = 117 \text{ m}$ is calibrated by regressing $(g/f)\Delta\text{SSH} = T_{\text{AX97}}/h$. The resulting transport derived using only surface velocity is in a good agreement with the observed one, with a correlation of 0.64 between $T_{\Delta\text{SSH}}$ and T_{AX97} , which is significant at 95% (Figure 4b).

iii Sverdrup method. We use the classic linear Sverdrup transport stream function to analyze the influence of the basin-wide WSC on the geostrophic variability of the BC at 22°S. The geostrophic transport stream function Ψ is determined by integrating the Sverdrup relationship zonally, starting from the eastern boundary x_E and is given by

$$\Psi(x) = -\frac{1}{\beta\rho_0} \int_{x_E}^x \hat{k} \cdot (\nabla \times \tau) dx \quad (3)$$

where β is the latitudinal gradient of f , $\rho_0 = 1,025 \text{ kg/m}^3$ is the reference density of the ocean, and τ is the wind stress. The BC closes the interior Sverdrup gyre and is defined as the maximum cumulative transport along the latitude of interest.

iv Ekman transport. The component of coastal upwelling due to Ekman transport is given by $W_{\text{ek}} = \tau_{\parallel}/(f\rho_0)$, where τ_{\parallel} is the component of the wind stress parallel to the coast, and its sign is defined as positive (upwelling) when the coast is on the right-hand side of the winds. The total upwelling volume

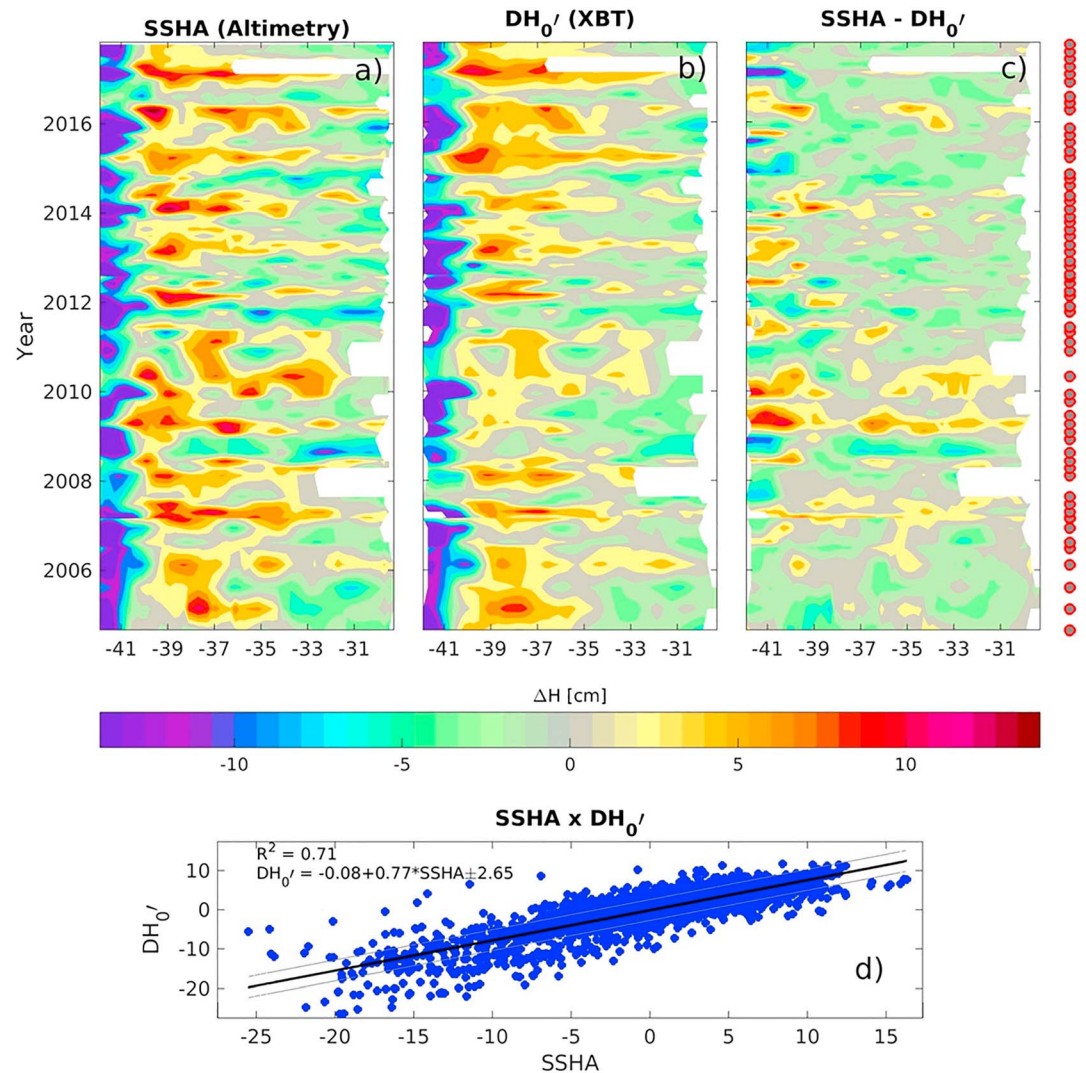


Figure 3. Comparison between the collocated SSHA and surface dynamic height along the AX97 high-density XBT transect. Hovmöller plots of the (a) SSHA, (b) demeaned surface dynamic height (DH_0'), and (c) $SSHA - DH_0'$. On the far right the location in time of the AX97 high-density XBT transect realizations. (d) The scatter plot SSHA against DH_0' and the linear regression between SSHA and DH_0' . DH = dynamic height; SSHA = sea surface height anomaly.

transport is calculated by first dividing by the cross-shore distance and then integrating W_{ek} over the area encompassed within 200 km offshore the South American coast.

2.2.4. Error Estimation of the BC Volume Transport

The velocity computation using XBT data is subject to uncertainties. According to Goes et al., (2015), the two largest uncertainties are associated with the salinity inference and the choice of reference level. We assess these two sources of uncertainty in the supporting information. This is performed using a bootstrap method. According to Figure S1, salinity uncertainties near 23°S generate a surface dynamic height uncertainty (standard error) of ~1 cm and velocity uncertainties going from zero at the reference level, where velocities are prescribed, to ~6.4 cm at the surface. The geostrophic reference level uncertainty is assessed by varying the reference depth from 300 m to 700 m at 50-m increments. The Argo/altimetry mean ADT is added to each selected depth, following the same methodology of section 2, producing a velocity standard error of ~1.33 cm/s using all sections. Using both uncertainties, the derived AX97 transport errors have a median value of 0.72 Sv. This value is added to the uncertainty of 0.92 Sv derived from the regression in Figure 4, for a total uncertainty of 1.64 Sv of the reconstructed transports.

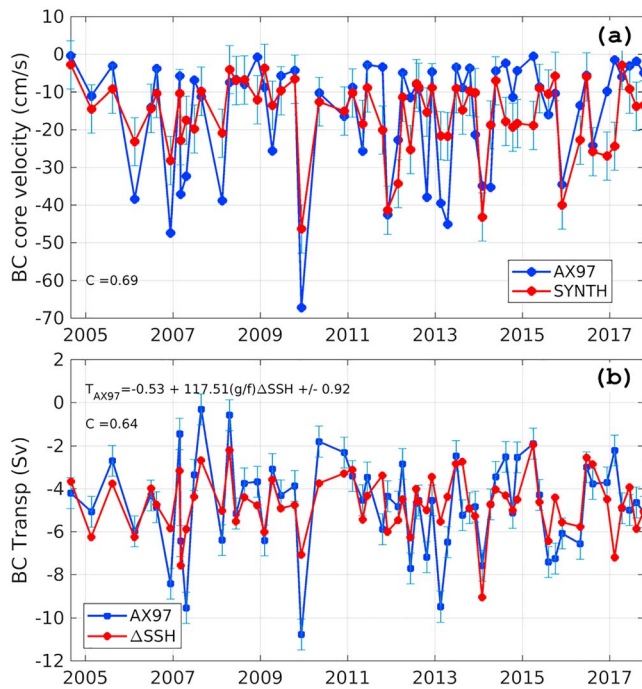


Figure 4. (a) BC core velocity and (b) BC volume transport calculated from the AX97 geostrophic velocities (blue) and derived from SSH data using the synthetic method (a) and the SSH gradient method fitted to have similar mean values (b). Also shown are the correlation coefficients estimated between the two time series in each panel and regression equation of the Δ SSH method on the top left of panel (b). The error bars in the AX97 core velocity and transport represent their estimated standard errors (see section 2.2.4 and supporting information). BC = Brazil Current; SSH = sea surface height.

3. Results

3.1. The Mean BC at 22°S

Using the AX97 XBT data, we define the main characteristics of the BC at 22°S. On average, the core velocity of the BC is -22 cm/s, and the BC is confined in the upper 550 m between 39°W and 41.5°W (Figures 5c and 5f). Below 550 m the signature of the Intermediate Western Boundary Current can be observed with approximate velocity of 5 cm/s. The mean ($\pm 1\sigma$) transport of the BC east of 40.9°W is 4.7 ± 1.9 Sv southward, similar to the earlier estimates ranging from 4.4 to 5.3 Sv (Evans et al., 1983). The transport standard deviation (± 1.9 Sv) is approximately half of the mean, showing the strong contribution from eddy variability to the BC (e.g., Lima et al., 2016; Soutelino et al., 2011). The shelf contribution, defined here as the region west of 40.9°W and shallower than 300 m, is of 0.9 ± 0.9 Sv, giving a total southward transport of 5.5 ± 1.7 Sv.

The mean temperature of the BC ranges from 22 to 24 °C (Figures 5a and 5d) and salinity from 36.8 to 37.2 psu in the top 75 m (Figures 5b and 5e), a signature of the salty and warm surface tropical waters. At the 75- to 450-m layer, a temperature of 13 to 22 °C and salinity of 35 to 36.7 psu characterize an almost linear T/S relationship of the South Atlantic Central Water (Figure S1), which is located between $\sigma_\theta = 25.8$ and 26.9 kg/m³ (Mémery et al., 2000). During the summer months, the signature of intensified upwelling is clear near the coastal area by the increased upward slope of isothermals/isohalines (Figures 5d and 5e). Due to the intensified summer upwelling, the BC core is shown further offshore ($\sim 40.5^\circ$ W; Figure 5f) relative to the winter average ($\sim 39.5^\circ$ W; Figure 5c). As the BC flows southward, more intense contributions of central and intermediate waters increase considerably its total transport. To quantify this contribution, we estimate the BC transport using the data from the AX18 XBT transect across the nominal latitude of 34.5°S (not shown; see companion paper Majumder et al., 2019). We apply the same methodology described

in section 2.2 for inner shelf extrapolation and Argo absolute dynamic height referencing at a 1,000 m. The mean BC transport across 34.5°S in the upper 1,000 m is 12.4 ± 3.5 Sv along 34.5°S, which is similar to the values calculated using other data and methods (Schmid & Majumder, 2018), which implies that the BC gains approximately 7–8 Sv of central and intermediate waters between 22°S and 34.5°S.

3.2. The Monthly Climatology of the BC Transport

As described in the previous section, the amplitude of variability ($\pm 1\sigma$) of the BC is comparable to the mean, due to its intense mesoscale activity along the western boundary. This implies that the seasonal cycle of the BC may be masked by the mesoscale variability, which constitutes a challenge to define its transport seasonal cycle (e.g., Vianna & Menezes, 2011). Figure 6 shows the monthly means of the BC transport using the AX97 data, as well as the transport derived from the two altimetry/XBT methods for the 2004–2017 period. Although there is indication that the BC transport is higher during the austral summer/fall (5.5 to 7 Sv) and weaker (2.5 to 4.0 Sv) in winter/spring, the seasonal cycle derived from the AX97 is noisy. The altimetry/XBT-derived methods provide a much smoother and well-defined seasonal cycle. The BC transport generated from these methods has similar means of 4.1 ± 1.7 Sv for the SSH gradient method and 4.6 ± 1.6 Sv for the synthetic method, which is also a feature of the higher temporal sampling.

The seasonal cycle of the BC transport estimated by the Sverdrup balance at 22.5°S shows a minimum of ~ 3 Sv during February–March and a maximum of ~ 8 Sv during June–September. Therefore, it is out of phase with the observed BC transport. The average Sverdrup stream function between 1992 and 2017 is negative (cyclonic) north of approximately 15°S, following the sign of the WSC, and becomes positive (anticyclonic) southward (Figure 7). The maximum WSC in the South Atlantic is located in the southeastern part of the basin, near the Agulhas retroflexion region (Figure 7). The maximum WSC region is stronger and further

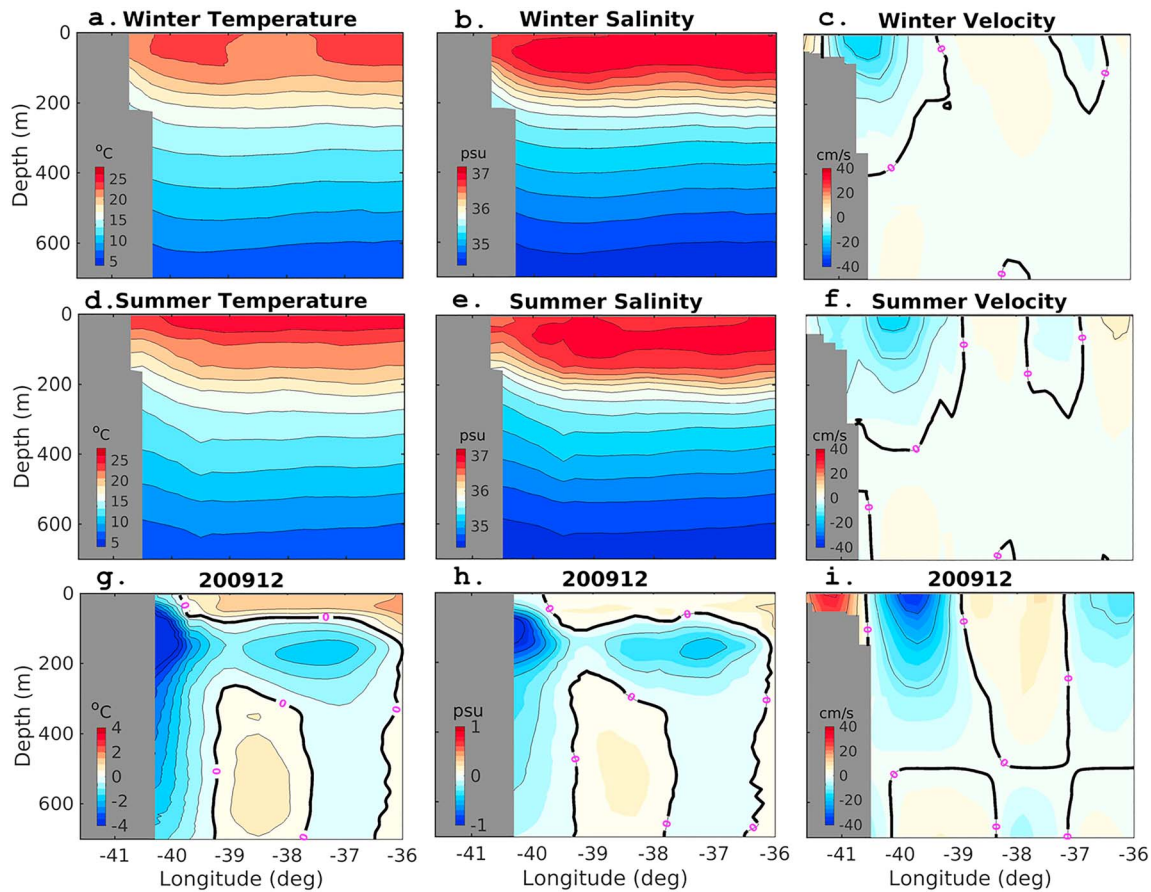


Figure 5. Mean climatological sections of temperature, salinity, and velocity for winter (a–c) and summer (d–f) months estimated using the AX97 high-density XBT transect data. Velocities are extrapolated to the shelf. (g–i) The anomalies relative to summer months for the section of December 2009.

South at approximately 39°S during summer (December–January–February, DJF), producing a stronger anticyclonic Sverdrup response (>50 Sv) near between 35°S and 40°S. During the winter (June–July–August), this WSC band migrates farther north, creating a maximum Sverdrup gyre response between 30°S and 38°S (Figure 7). Consequently, the difference between winter and summer (June–July–August–DJF) shows a weakening of the WSC south of 35°S during winter and WSC strengthening between 35°S and 15°S, resulting in a stronger winter Sverdrup transport across 22.5°S (Figure 6). The incompatibility between the seasonal cycle of the stationary linear Sverdrup model and upper-ocean western boundary currents can be explained by two main causes: (i) the time lag of the baroclinic adjustment via Rossby wave propagation and (ii) remote versus local wind forcing.

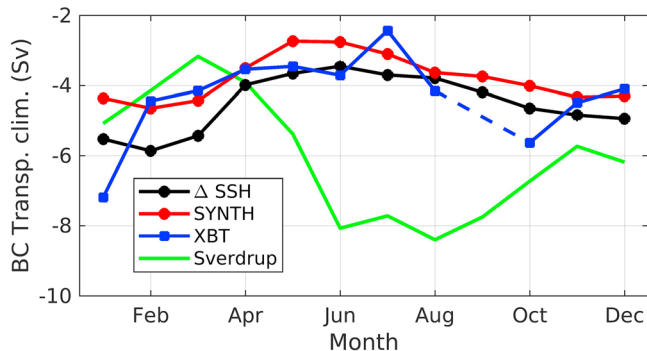


Figure 6. Monthly averages of BC transport at 22°S for the SSH gradient method (black), synthetic method (red), from AX97 high-density XBT data (blue), and Sverdrup transport (green). No AX97 observations are available in September (blue dashed line). All monthly climatology values are calculated for the period between 2004 and 2017. BC = Brazil Current; SSH = sea surface height.

To further investigate the seasonal oceanic variability of along 22.5°S, Figure 8 displays the longitude–time diagrams of SST, SSH, WSC, and meridional wind stress (TAUY) monthly climatologies. SST and SSH (Figures 8a and 8b) show similar behavior along 22.5°S, with maximum values of SST and SSH from February to April, intensification west of 20°W, and minimum values from August to October. Beal et al. (2013) described a semiannual Rossby wave propagation across the Arabian Sea, which would be potentially responsible for a seasonal phase shift along the western boundary. In Figure 8b, no SSH propagation is visible throughout the year, from which we can infer that the annual large-scale adjustment is not the cause of the shift between the integrated WSC and the BC. Semiannual Rossby

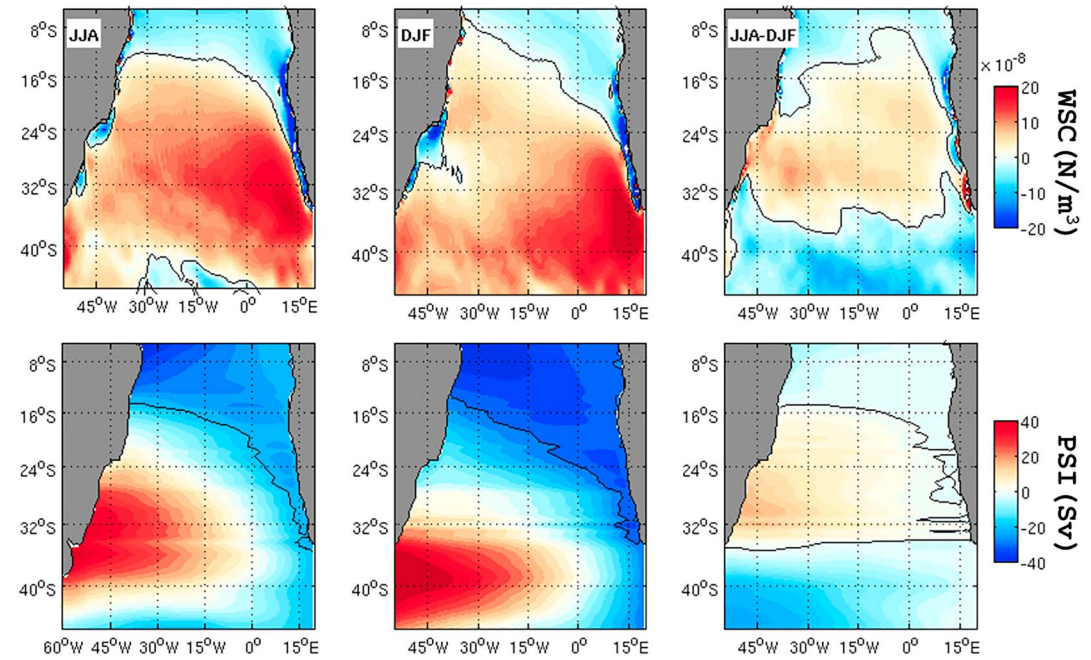


Figure 7. Seasonally averaged wind stress curl (10^{-8} N/m^3 , upper panels) and associated Sverdrup transport (Sv, lower panels) in the South Atlantic sector. Panels show average from June-July-August (JJA, left column), December-January-February (DJF, middle column), and JJA-DJF (right column). WSC = wind stress curl.

waves are also found in the South Atlantic (Polito & Liu, 2003), but as in the Indian Ocean, they often have the largest amplitudes in the tropics. At this latitude, the WSC is indeed stronger in the basin interior from June to September (Figure 8c), with its maximum located between 20°W and 5°E . West of 30°W , it is the southward component of the wind stress that is most intense during the summer (DJF) months (Figure 8d), whose alongshore component is associated with the increased summer coastal upwelling in Cabo Frio. Therefore, the local component of the wind may be the strongest forcing of the seasonality of the BC. Using a reduced gravity model, Rodrigues et al. (2007) suggested that it is the local WSC and not the remote forcing (i.e., westward propagation of anomalies) that impacts the seasonal variability of upper thermocline flow along the western boundary and on the South Equatorial Current bifurcation ($\sim 10\text{--}15^\circ\text{S}$).

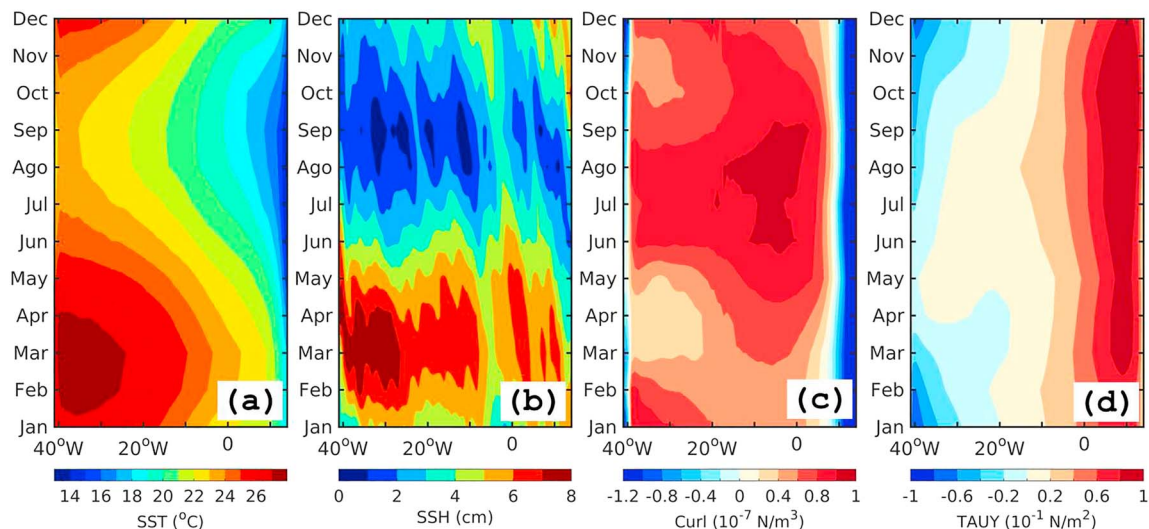


Figure 8. Monthly averages between 18°S and 23°S of (a) SST, (b) SSH, (c) wind stress curl, and (d) meridional wind stress. SST = sea surface temperature; SSH = sea surface height.

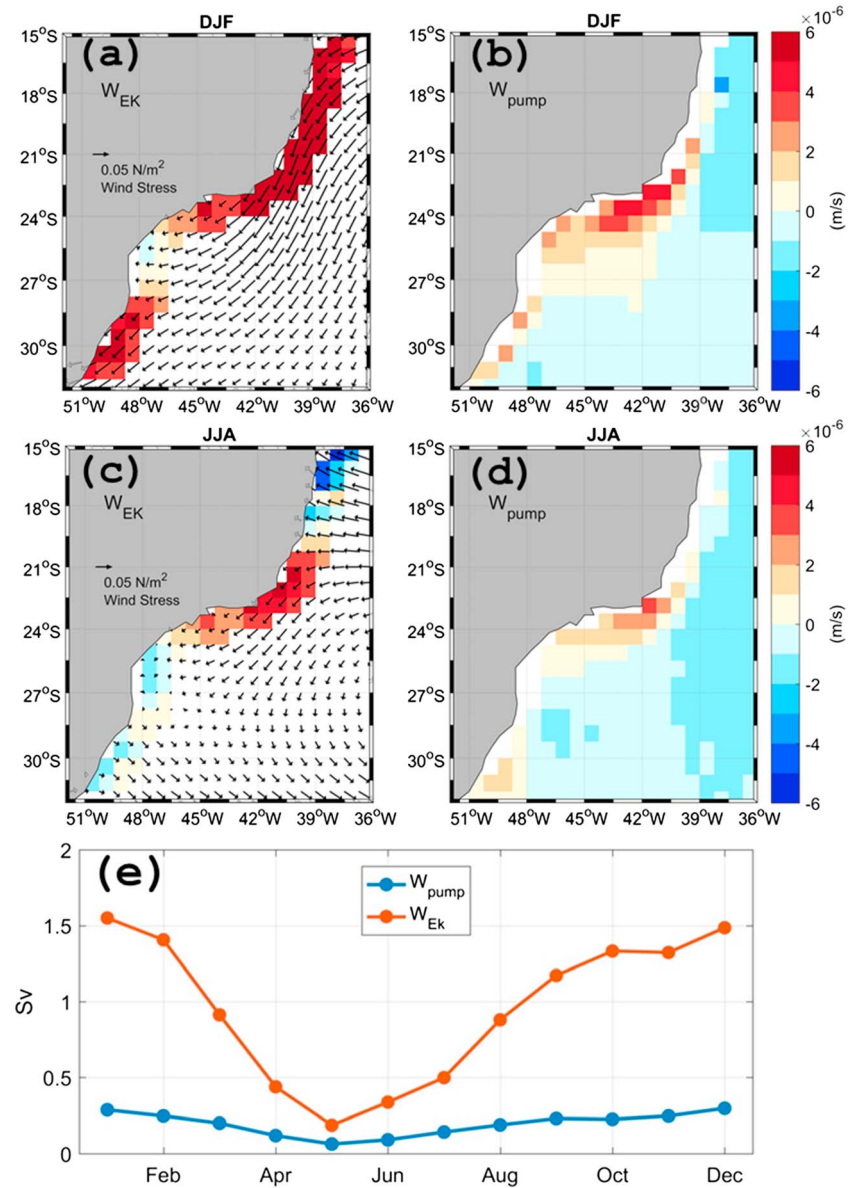


Figure 9. Ekman transport (a, c) and Ekman pumping (b, d) velocity (m/s) calculated off the western South Atlantic coast for austral summer (a, b) and winter (c, d). Black arrows in (a, c) are the wind stress vectors. (e) Monthly averaged transport of Ekman pumping (W_{pump}) and coastal Ekman transport (W_{ek}) integrated across 200 km from the coast between 18°S and 25°S . DJF = December-January-February; JJA = June-July-August.

The effect of the seasonality of the alongshore wind and near coastal WSC on the upwelling is shown in Figure 9. Similar to what was shown in Castelao and Barth (2006), due to the prevailing southwestward direction of the winds, coastal upwelling and Ekman pumping occur all year-round but are stronger during summer months. The vertical transport associated to Ekman transport is approximately 3 times stronger than the Ekman pumping calculated within 200 km of the coast. The seasonality of the coastal upwelling and Ekman pumping near the western boundary (Figure 9e) follows the same seasonality of the BC transport. The dynamic relation between the BC variability and the coastal upwelling will be explored in the next section.

3.3. The Interannual Variability of the BC and Associated Forcings

Although there are substantial differences between the seasonal cycles of the transports calculated using altimetry-based and the XBT estimates, there is strong agreement between the daily time series of the

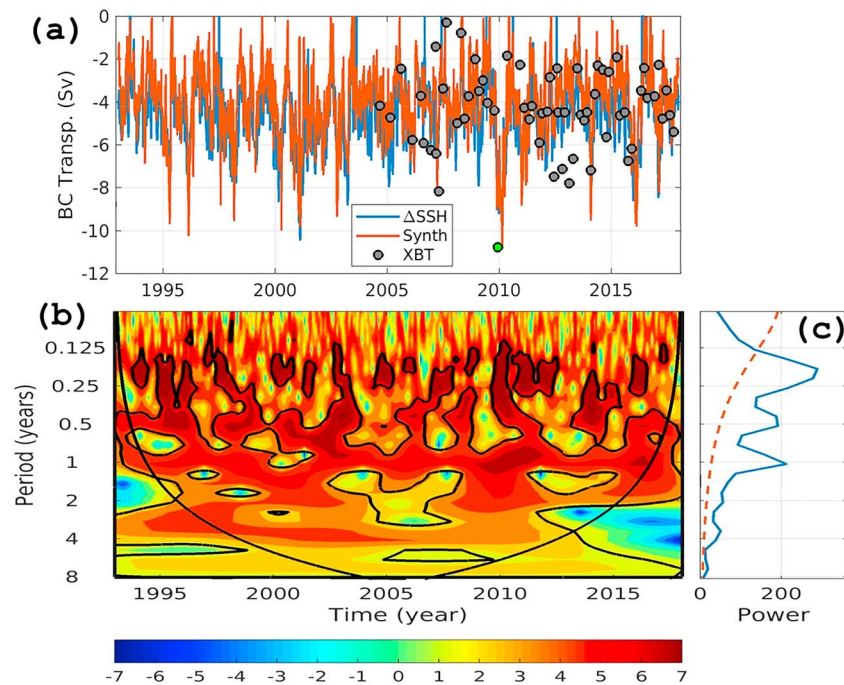


Figure 10. (a) Reconstructed time series of the BC transport using the SSH gradient method (blue), the synthetic method (red), and the transport estimated for the AX97 high-density XBT transects (gray dots). The 2009–2010 event measured by the AX97 is highlighted as a green dot. (b) Wavelet map showing the power spectrum of the synthetic transport (red) relative to time and periods. Color bar shows the log₂ values of energy. (c) Global spectrum of the wavelet decomposition (blue) with respective significance level (dashed red). BC = Brazil Current; SSH = sea surface height.

reconstructed BC transport with those from the XBT realizations (Figure 10a). This reinforces the idea that the seasonal cycle of the BC transport derived from XBT data has still not converged to a true mean value due to weak signal-to-noise ratio. Between the two reconstructed daily time series, the correlation is above 0.95, which suggests that both methods can reproduce the variability of the BC transport. It is noteworthy to mention that these two methods use different calibration and different ways to define the eastern limit of the BC used in the integration of the volume transport (see section 2.2.3). The two methods have their advantages, the Δ SSH is easier to apply, and SYNTH gives velocity structure information over depth. The fact that these transport values are so similar shows that these estimates are robust.

The wavelet spectrum analysis (Liu et al., 2007) is used to decompose the variability of the synthetic BC transport time series. The SYNTH time series shows significant variability from mesoscale to decadal timescales (Figure 10b), since it is reconstructed from 25 years of daily altimetry data. Note, however, that the mean effective spatial and temporal resolutions of the DUACS product are estimated to be \sim 200 km and \sim 28 days period, respectively (Ballarotta et al., 2019). The most prominent timescales are the annual and semiannual cycles (e.g., Figure 6), in addition to large amplitude eddy variability below 100 days. A statistically significant interannual variability of the order of 2–4 years can also be identified. No significant trend is observed in the reconstructed time series of the BC at this latitude since 1993.

To determine if and how the interannual variability of the BC is driven by the Sverdrup dynamics, we compute the lag correlation between the anomalies of the synthetic BC transport time series and the anomalies of the western boundary transport derived from the linear Sverdrup balance. Both time series were previously smoothed with a 7-month rectangular filtering to focus on interannual variability. The maximum correlation of $r = 0.32$ is reached when the BC transport lags the Sverdrup transport by 19 months (Figures 11a and 11b). Although modest, this correlation is statistically significant at the 95% level, calculated using a two-tailed Student's t distribution and a reduced number of degrees of freedom approximated from its sample autocorrelation function. The baroclinic adjustment of the ocean circulation to WSC forcing is determined primarily by the westward propagation of first baroclinic mode Rossby waves (Chelton & Schlax, 1996). Using the method of Barron et al. (2009), we estimate an optimal propagation speed of 5.3 ± 0.8 cm/s

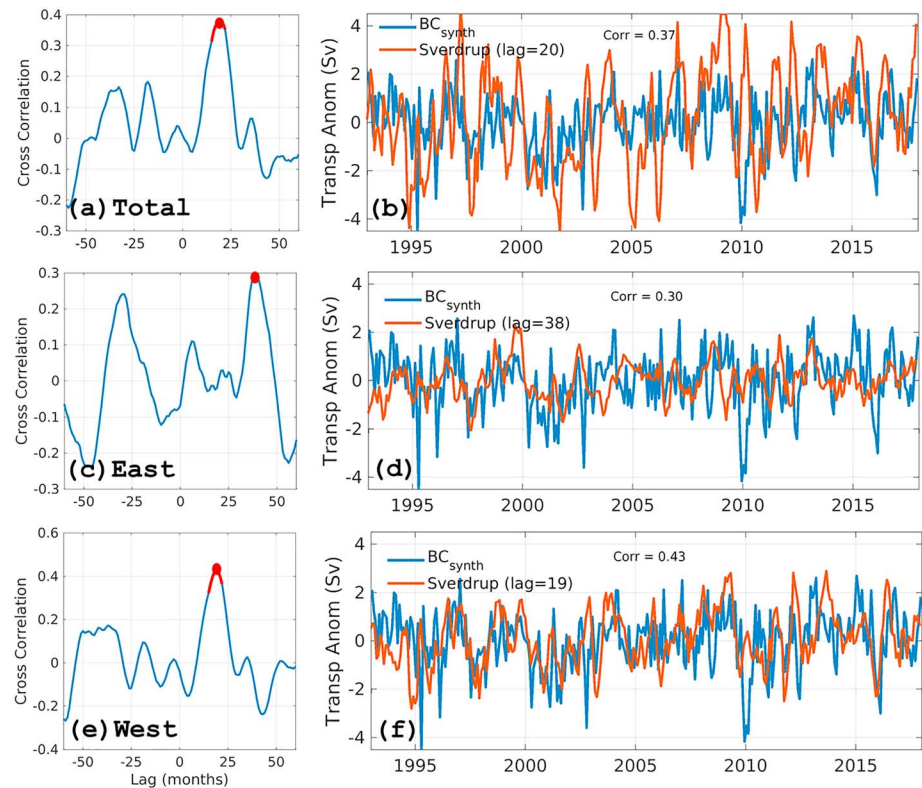


Figure 11. Relationship between 7-month smoothed monthly anomalies of BC transport and Sverdrup transport at 22.5°S. (left column) Lagged correlations between BC and Sverdrup transport anomalies for (a) total (40°W to 15°E), (b) east (0 to 15°E), and (c) west (40°W to 18°W). Positive lags mean Sverdrup leads; red contour represents the values that are significant at the 95% level using a student's *t* test, and red dots are the locations of maximum correlations. (right column) Anomalous time series of BC transport (blue) and the Sverdrup transport (red) lagged in time by the number of months of the maximum correlation found in the left panels for (b) total, (d) east, and (f) west. The values of maximum correlation and their lags are displayed in the figures. BC = Brazil Current.

of the unfiltered SSHA data along 22.5°S. This estimate is consistent with a first baroclinic Rossby wave radius of about 50 km, as well as with previously estimated westward phase speeds for this latitude between 3 and 6 cm/s (Chelton & Schlax, 1996). However, this would provide a timescale for westward propagation across the approximate 6,000 km width of the basin of 4–5 years, which is much longer than the 20-month period shown in Figure 11a.

Similar to the work of DiNezio et al. (2009) for the Florida Current, we breakup the Sverdrup transport into contributions from the west (SvW, 40–18°W) and east (SvE, 0–15°E) parts of the basin (Figures 11d and 11f). Following the same methodology, a lagged correlation is applied between the BC and the Sverdrup contributions (Figures 11c and 11e). The maximum correlation between the BC transport and SvE is $r = 0.30$ at 38-month lag, which is expected given the larger distance traveled from the eastern WSC source to the western boundary. Despite the fact that the time lag response of the BC to the WSC forcing is more consistent with the baroclinic Rossby adjustment, the correlation between SvE and the BC is reduced and is not statistically significant. As opposed to SvE, the correlation from the western contribution of the WSC increased to $r = 0.43$ (Figures 11e and 11f), and the lag remained approximately the same (19 months) as the correlation to the basin-wide WSC. These results suggest that the western part of the basin dominates the Sverdrup response to the BC. In addition, the unequivocal agreement between the interannual variability of the BC transport and the WSC in the western side of the basin (Figure 11f) can partially explain the phase difference to the observed seasonal cycle of the BC in Figure 6. However, it still does not explain much of the intraannual variability such as the strong transport anomaly in the summer of 2009/2010.

The lifting of the thermocline along the coast by upwelling favorable winds is associated with a trough in sea level near the coast and increase in sea level offshore (Gill & Clarke, 1974; Csanady, 1982) in scales of

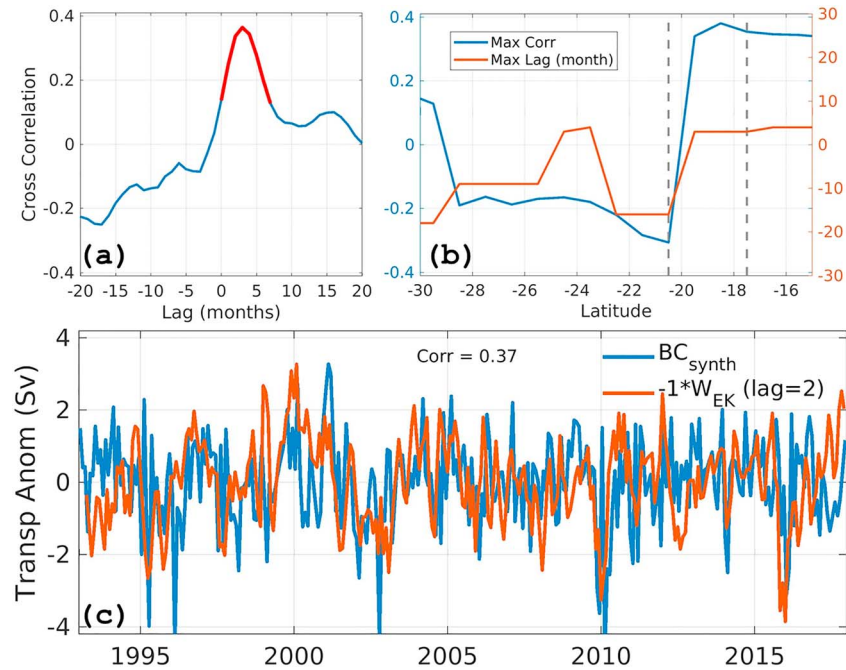


Figure 12. Comparison between BC transport at 22.5°S and coastal Ekman transport (W_{ek}). (a) Lagged correlation between BC transport and W_{ek} averaged between 19°S and 21°S. Thicker red line is the 95% confidence interval from a student's t -test. (b) Maximum correlation (blue) and monthly lag of maximum correlation between BC transport and W_{ek} . (c) Time series of BC transport (blue) and 2-month lagged W_{ek} (red). W_{ek} is multiplied by -1 to agree with stronger transport to the south. BC = Brazil Current.

approximately 1 month (Thompson, 1986), potentially increasing the BC transport by enhancing the cross stream pressure gradient. We reconstruct the time series of anomalies of coastal Ekman transport divergence along the western boundary region and compare it to the synthetic reconstruction of the BC transport (Figure 12). The anomalous time series are filtered with a 3-month rectangular window to reduce noise and eddy variability. The lagged correlation between the W_{ek} and BC transport time series (Figure 12b) reaches its maximum upstream of the BC path, between 15°S and 21°S. Aguiar et al. (2014) showed that W_{ek} controls most of the upwelling events between 17°S and 21°S, and W_{pump} plays a secondary role. Thus, an index for the coastal upwelling near AX97 is constructed by averaging W_{ek} between 17°S and 21°S, from which a correlation of $r = 0.37$ (significant at 95%) is found with the BC when the wind leads by 2 months (Figure 12a). These results suggest that the upwelling associated with the alongshore winds upstream of the BC path cause a baroclinic response, leading the BC flow within 2 months. The two strongest upwelling events are for December 2009 and January 2016. One such event was captured by the XBT data during December 2009, when an upwelling response is associated with a stronger BC (Figure 12b). This is perhaps the strongest event recorded with this data. It is observed that the strong upwelling lowers the temperatures, salinity, and sea level along the coast (Figures 5g–5i). Next, the summer 2009/2010 event is investigated in more detail.

3.4. The 2009–2010 Warm Event and Regional Impacts

Figure 13 shows that during the austral summer of 2009/2010, there was a strong anomaly of the BC, in which the BC transport increased to ~ 11 Sv (green dot in Figure 10), approximately 2.5 times its average value. The AX97 section from December 2009 (Figure 5i) shows the BC core speed of 70 cm/s, 40 cm/s stronger relative to the austral summer average of 30 cm/s (Figure 5f). At this time, anomalous upwelling in the Cabo Frio region is also visible from the XBT data, and the isothermal depths are much shallower than the seasonal average close to the boundary (Figure 5d), producing a cooling of up to 4 °C (Figure 5g). The anomalous event of summer 2009/2010 was characterized by SST anomalies in the western South Atlantic that reached 3 °C (Figure 13), which in the study period is the strongest marine heat wave in the AX97 location.

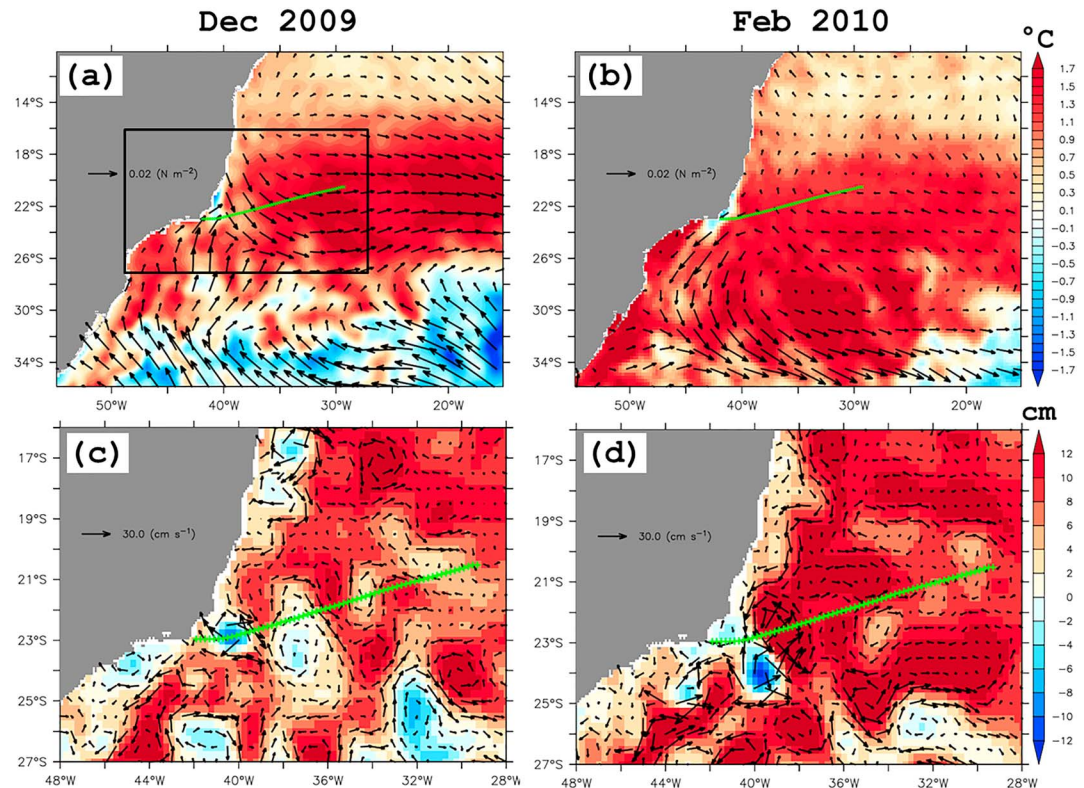


Figure 13. Monthly averaged anomalies of sea surface temperature ($^{\circ}\text{C}$) and wind stress (N/m^2) for (a) December 2009 and (b) February 2010 and sea surface height anomaly (cm) and surface geostrophic velocities (cm/s) for (c) December 2009 and (d) February 2010. The AX97 reference transect is overlaid in green. Panels (c) and (d) are shown in a reduced domain shown as a black box in panel (a) to emphasize the western boundary region.

The SST anomalies were located in the center of the basin between 20°S and 22°S in November, which according to Rodrigues et al. (2015) were generated as a response in the South Atlantic to a moderate to strong Central Niño event in the Pacific. From 20°S to 22°S , these anomalies appeared to migrate further south in February toward 30°S – 32°S . Strong anticyclonic wind stress anomalies were observed around the maximum of the warm SST anomaly, whose alongshore component favors an increased upwelling response, first around 15°S – 18°S and further south in February. Offshore SSH was also increased during the event (Figures 13c and 13), following the regions of increased SST. From the SSHA maps in Figures 13c and 13d, it is observed a stationary eddy near 40°W along the XBT transect, generating a trough in sea level of more than 10 cm throughout the 3-month period. This is the so-called Sao Tome eddy, a semipermanent cyclonic feature that develops in the region and can be originated from a detachment of a BC meandering (Calado et al., 2008; Campos et al., 2000; Lima et al., 2016). Therefore, our results suggest that in the summer 2009/2010, a mix of positive SSH anomalies propagated westward, anticyclonic wind anomalies facilitating the coastal upwelling and decreasing the coastal sea level, and a stationary eddy near 40°W along the XBT transect contributed for the strong BC anomaly in that period.

Figure 14 shows the contribution of the sea level anomalies to the BC transport separated into inshore [41°W , 40°W] and offshore [40°W , 38°W] regions. Near the coast (Figure 14a), the SSH (DH) anomalies reached between 15 and 20 cm in late 2009, which characterizes the highest sea level anomaly in the whole time series, and it is linked to the strong coastal upwelling anomaly and also the influence of the stationary eddy attached to it. Offshore (Figure 14b), the AX97 time series does not show strong anomalies in 2009/2010, which corroborates with the pattern shown in Figure 5 of the compensation of warm upper 100-m depth anomalies by a cooling underneath. A strong positive anomaly of ~ 15 cm is, however, detected by the daily altimetry data along the reference transect (thin gray line) during early February 2010, which is associated to a thermosteric response to the warm anomaly approaching the coast. Similar offshore warm

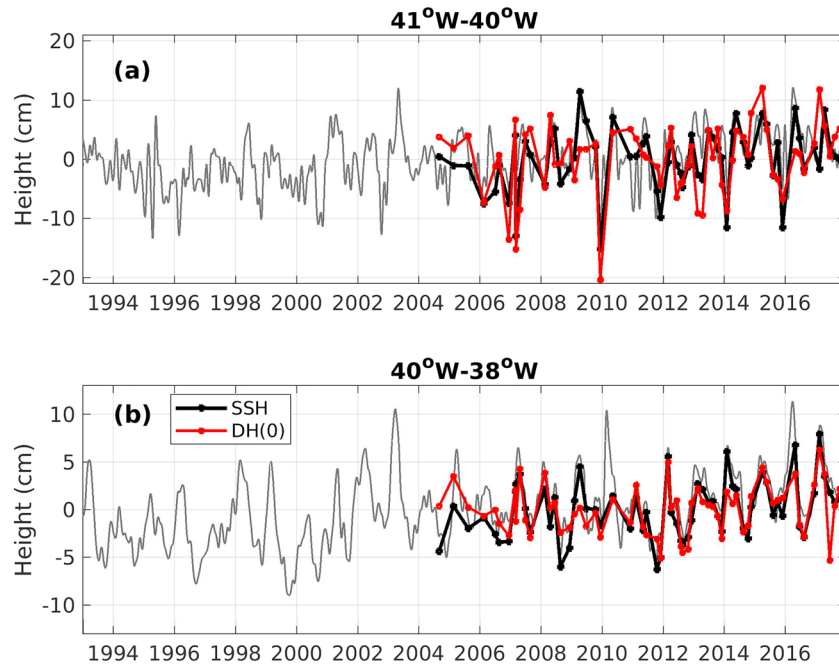


Figure 14. Comparison between altimetric SSH (black) and DH(0) from XBT data (red) time series calculated along the AX97 sections. The thin gray line is the daily SSH with a 61-day low-pass Hanning filter, along the mean AX97 transect for the entire altimetric period. SSH and DH are averaged in two regions: (a) near the coast (41°W to 40°W) and (b) offshore (40°W to 38°W). SSH = sea surface height; DH = dynamic height.

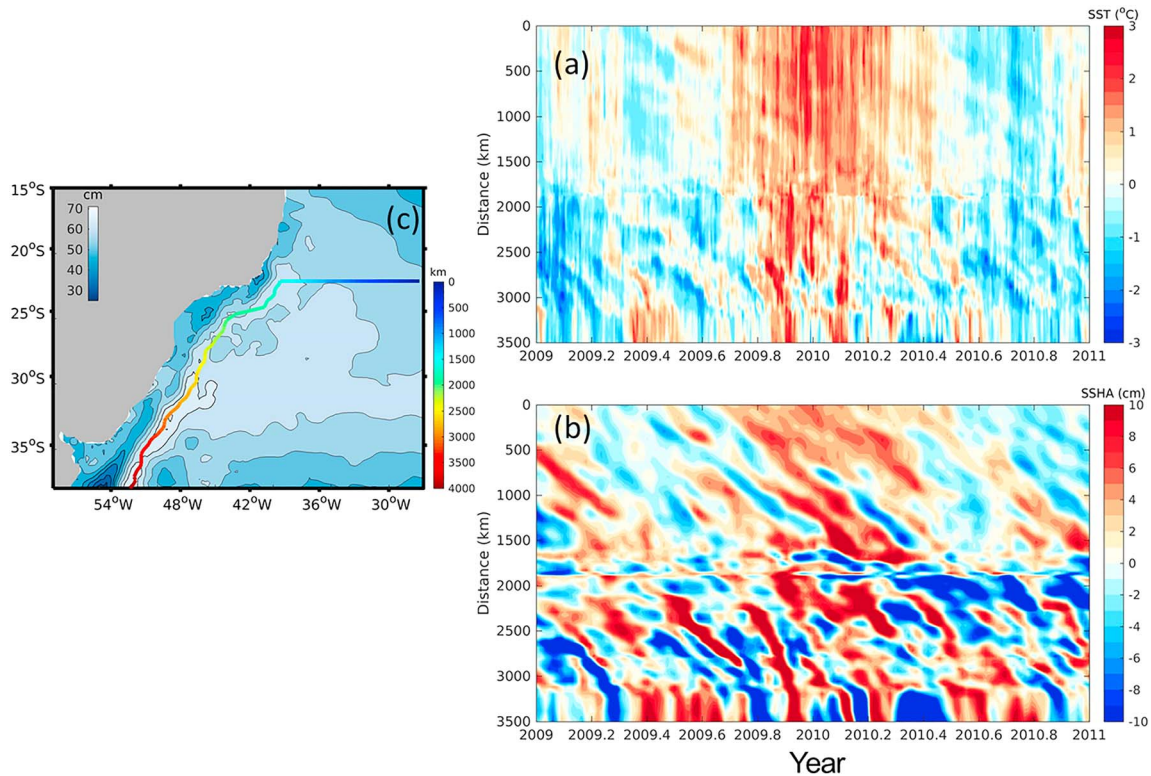


Figure 15. Distance-time plots of daily anomalies (2000–2015 first and second harmonics subtracted) of (a) SST and (b) SSH (bottom) between 2009 and 2011. Regional map on panel (c) shows the bottom topography (contours) overlaid by the distance path (colored line in kilometers) along the 22°S and off the South American coast along the southward path east of the Brazil Current used in the Hovmoller plot panels. SST = sea surface temperature; SSH = sea surface height.

anomalies are also observed during late March 2003 and in January 2016 (Figure 14b), with smaller amplitudes.

To investigate how the SST and SSH anomalies propagate toward and along the coast during the 2009/2010 event, a Hovmöller plot is produced following the interior path toward the coast along 22°S and continuing along the BC path from 22°S to 37°S (Figure 15). Positive SSH anomalies propagate 1,000 km from 30°W of the basin toward the coast along 22°S for about 3 months (Figure 15b), whereas SST anomalies do not show the same propagation pattern as SSH (Figure 15a). This is expected, since SST anomalies in the WSSA region are strongly influenced by atmospheric features both locally and remotely (e.g., Rodrigues & Woollings, 2017). After reaching the BC, a southward propagation path of SSH anomalies is also visible, although aliased by strong mesoscale variability typical of the region. These results suggest that the increased heat transport along the BC and its propagation timescales during this event were mostly driven by velocity anomalies rather than temperature anomalies. Effects of planetary Rossby wave propagation at different latitudes (Majumder et al., 2019; Polito & Liu, 2003) and convergence associated with the meridional overturning circulation (Lopez et al., 2016) may also play an important role for the increased heat anomaly within the subtropical gyre, but this is beyond the scope of this study.

4. Conclusions

In the present study, the AX97 high-density XBT data are used along with satellite altimetry and Argo-based absolute dynamic topography to reconstruct the geostrophic velocity of the BC across 22°S. The reconstructed velocity includes the shelf and mesoscale components. A time series of the BC transport is reconstructed since 1993 using two methods, one using synthetic velocities (Goes et al., 2013) and the other using only surface velocity from altimetry calibrated to the transport from the XBT data. The two methods show very strong agreement and correlation above 0.9. The reconstructed BC shows a well-defined seasonal cycle with a stronger transport (5–7 Sv) from January to March and a weaker transport (2 Sv) during August–September. The seasonal variability was reasonably well captured by the 62 transects of the XBT data, although still subject to some noise due to strong eddy variability of the BC. The integrated WSC across the basin is out-of-phase with the seasonal cycle of the BC transport. The WSC is stronger during the austral winter and in the central and western part of the basin. This suggests that there is delayed adjustment time to the WSC via baroclinic adjustment, and also contributions from the coastal upwelling to the BC variability, which is stronger during summer.

At interannual timescales, the variability of the BC agrees with the variability of the large-scale WSC in the western side of the basin, with a correlation of 0.43 when the winds lead the BC by 19 months. Therefore, it can be linked to the baroclinic adjustment of the subtropical gyre via Rossby wave mechanisms (e.g., Majumder et al., 2019; Häkkinen et al., 2013). In addition, the BC interannual variability shows a statistically significant ($r = 0.37$) relationship with the upwelling north of the AX97 transect (15°S to 21°S), and with a 2-month delay, which can be associated to the advection of anomalies downstream (e.g., Enfield & Allen, 1980), as detected by the cooling of 4 °C the BC down to 400 m in December 2009. Other processes may influence the variability of the BC transport, such as mesoscale eddies, coastally trapped waves, and interaction of the bathymetry with the flow.

During the event of summer 2009/2010, the BC transport increased threefold, reaching ~11 Sv for 3 months. This event was concomitant with the 2009–2010 central Niño event (Xue et al., 2011), which influences the South Atlantic variability via atmospheric Rossby wave teleconnections, which follows primarily to the Pacific–South American pattern (e.g., Ashok et al., 2007; Mo & Paegle, 2001), and the development of a positive phase of the South Atlantic dipole (Rodrigues et al., 2015). Therefore, strong positive SST anomalies of ~3 °C, the highest in the region for the period of study, developed in the center of the basin in October/November 2009 and propagated westward along ~20°S. Positive SSH anomalies were detected offshore of the AX97 transect in early February 2010. The SST anomalies were associated with an anomalous anticyclonic wind pattern, resulting in increased coastal upwelling north of 22°S. The increased upwelling decreased the coastal sea level by 15 to 20 cm, partly driven by the cooling of the water column detected by the XBT data in December of 2009, which also increased the SSH gradient across the AX97 section and the meandering of the BC. The increased BC meandering may have caused a stationary eddy growth, as

suggested by previous studies (e.g., Aguiar et al., 2014; Calado et al., 2010), which occupied the AX97 location for nearly 3 months and also contributed for the decreased sea level near the coast.

SSH anomalies were advected to and along the BC path, setting the timescale of approximately 2 months for the propagation of the SST anomalies reaching the so-called western subtropical South Atlantic region (henceforth WSSA; 50°W–20°W and 25°S–35°S). The BC defines the pathway of the warm waters southward in the South Atlantic and therefore is an important part of the Atlantic meridional overturning circulation. In addition, positive SST anomalies in the WSSA region are associated with weaker South Atlantic Convergence zone and potentially droughts in the Southeast Brazilian coast, a highly populated region. Further investigation using numerical models may be necessary to ascertain the proper mechanisms that relate the role of the BC on the regional climate and extreme events.

Significant long-term trends were not detected in the reconstructed BC transport. Recent studies using model outputs show a tendency for the Southern Hemisphere boundary currents to strengthen due to the tropical expansion and stronger winds (e.g., Pontes et al., 2016, Yang et al., 2016). Further south, there are indications of a southward migration of the Brazil-Malvinas Confluence but can be driven by a weakening of the Malvinas Current and a southward shift of the westerly winds (Combes & Matano, 2014; Wu et al., 2012). In this case, it is possible that there is low latitudinal coherence of the BC, or a deepening of the BC instead of strengthening, and it may have not been detected by the present methodology.

Acknowledgments

Argo derived climatological absolute dynamic topography was downloaded at Asia-Pacific Data-Research Center (APDRC) website (<http://apdrc.soest.hawaii.edu/>). The ERA-Interim wind stress data are available online (<https://www.ecmwf.int>). The Reynolds SST data are available online (<https://www.esrl.noaa.gov>). AVISO data are available at the Copernicus Marine and Environment Monitoring Service center (<http://marine.copernicus.edu>). The AX97 high-density XBT transect is available online (<http://www.aoml.noaa.gov/phod/hdenxbt>). The authors would like to thank the logistical support provided by the Brazilian Navy Hydrographic Office (DHN) and the Brazilian GOOS Program as well as the financial funding provided by the Brazilian Research Council (CNPq) and Ministry of Science, Technology, Innovation and Communications (MCTIC). We also thank Ricardo Domingues, Tiago Bilo, Sang-Ki Lee, and Gustavo Goni for suggestions in the manuscript and NOAA AOML and NOAA Climate Program Office for support. This work is funded by the National Science Foundation (NSF) grant 1537769. This research was carried out under the auspices of the Cooperative Institute for Marine and Atmospheric Studies (CIMAS), a NOAA cooperative institute hosted at the University of Miami under the Cooperative Agreement NA15OAR4320064.

References

- Aguiar, A. L., Cirano, M., Pereira, J., & Marta-Almeida, M. (2014). Upwelling processes along a western boundary current in the Abrolhos-Campos region of Brazil. *Continental Shelf Research*, *34*, 42–59. <https://doi.org/10.1016/j.csr.2014.04.013>
- Artana, C., Ferrari, R., Koenig, Z., Sennéchaël, N., Saraceno, M., Piola, A. R., & Provost, C. (2018). Malvinas Current volume transport at 41°S: A 24 yearlong time series consistent with mooring data from 3 decades and satellite altimetry. *Journal of Geophysical Research: Oceans*, *123*, 378–398. <https://doi.org/10.1002/2017JC013600>
- Ashok, K., Behera, S. K., Rao, S. A., Weng, H., & Yamagata, T. (2007). El Niño Modoki and its possible teleconnection. *Journal of Geophysical Research*, *112*, C11107. <https://doi.org/10.1029/2006JC003798>
- Assad, L. P., Böck, C., Candella, R., & Landau, L. (2015). Influence of El Niño wind stress anomalies on South Brazil Bight ocean volume transports. *International Journal of Oceanography*, *2015*, 1–15. <https://doi.org/10.1155/2015/965314>
- Ballarotta, M., Ubelmann, C., Pujol, M.-I., Taburet, G., Fournier, F., Legeais, J.-F., et al. (2019). On the resolutions of ocean altimetry maps. *Ocean Science Discussions*. <https://doi.org/10.5194/os-2018-156> in review
- Barron, C. N., Kara, A. B., & Jacobs, G. A. (2009). Objective estimates of westward Rossby wave and eddy propagation from sea surface height analyses. *Journal of Geophysical Research*, *114*, C03013. <https://doi.org/10.1029/2008JC005044>
- Beal, L. M., Hormann, V., Lumpkin, R., & Foltz, G. R. (2013). The response of the surface circulation of the Arabian Sea to monsoonal forcing. *Journal of Physical Oceanography*, *43*(9), 2008–2022. <https://doi.org/10.1175/JPO-D-13-033.1>
- Biló, T. C., da Silveira, I. C. A., Belo, W. C., de Castro, B. M., & Piola, A. R. (2014). Methods for estimating the velocities of the Brazil Current in the pre-salt reservoir area off southeast Brazil (23°S–26°S). *Ocean Dynamics*, *64*(10), 1431–1446. <https://doi.org/10.1007/s10236-014-0761-2>
- Calado, L., da Silveira, I. C. A., Gangopadhyay, A., & de Castro, B. M. (2010). Eddy-induced upwelling off Cape Sao Tomé (22°S, Brazil). *Continental Shelf Research*, *30*(10-11), 1181–1188. <https://doi.org/10.1016/j.csr.2010.03.007>
- Calado, L., Gangopadhyay, A., & da Silveira, I. C. A. (2006). A parametric model for the Brazil Current meanders and eddies off southeastern Brazil. *Geophysical Research Letters*, *33*, L12602. <https://doi.org/10.1029/2006GL026092>
- Calado, L., Gangopadhyay, A., & da Silveira, I. C. A. (2008). Feature-oriented regional modeling and simulations (FORMS) for the western South Atlantic: Southeastern Brazil region. *Ocean Modelling*, *25*(1-2), 48–64. <https://doi.org/10.1016/j.ocemod.2008.06.007>
- Campos, E. J. D., Velhote, D., & da Silveira, I. C. A. (2000). Shelf break upwelling driven by Brazil Current cyclonic meanders. *Geophysical Research Letters*, *27*(6), 751–754.
- Carrere, L., Lyard, F., Cancet, M., Guillot, A., Picot, N., et al. (2016). FES 2014, a new tidal model - Validation results and perspectives for improvements. (Poster) *Living Planet Symposium, Prague*, 9–13 <http://lps16.esa.int>.
- Carrere, L., & Lyard, F. (2003). Modeling the barotropic response of the global ocean to atmospheric wind and pressure forcing - comparison with observations. *Geophysical Research Letters*, *30*(6), 1275. <https://doi.org/10.1029/2002GL016473>
- Carvalho, L. M., Jones, C., & Liebmann, B. (2004). The South Atlantic convergence zone: Intensity, form, persistence, and relationships with intraseasonal to interannual activity and extreme rainfall. *Journal of Climate*, *17*(1), 88–108. [https://doi.org/10.1175/1520-0442\(2004\)017<0088:TSACZI>2.0.CO;2](https://doi.org/10.1175/1520-0442(2004)017<0088:TSACZI>2.0.CO;2)
- Castelao, R. M., & Barth, J. A. (2006). Upwelling around Cabo Frio, Brazil: The importance of wind stress curl. *Geophysical Research Letters*, *33*, L03602. <https://doi.org/10.1029/2005GL025182>
- Chelton, D. B., & Schlax, M. G. (1996). Global observations of oceanic Rossby waves. *Science*, *272*(5259), 234–238. <https://doi.org/10.1126/science.272.5259.234>
- Chelton, D. B., Schlax, M. G., & Samelson, R. M. (2007). Summertime coupling between sea surface temperature and wind stress in the California current system. *Journal of Physical Oceanography*, *37*(3), 495–517. <https://doi.org/10.1175/JPO3025.1>
- Combes, V., & Matano, R. P. (2014). Trends in the Brazil/Malvinas confluence region. *Geophysical Research Letters*, *41*, 8971–8977. <https://doi.org/10.1002/2014GL062523>
- Costa, V. S., Mill, G. N., Gabioux, M., Grossmann-Matheson, G. S., & Paiva, A. M. (2017). The recirculation of the intermediate western boundary current at the Tubarão Bight-Brazil. *Deep Sea Research Part I: Oceanographic Research Papers*, *120*, 48–60. <https://doi.org/10.1016/j.dsr.2016.12.001>

- Csanady, G. T. (1982). *Circulation in the Coastal Ocean* (279 pp. Springer.
- da Silveira, I., Lima, J., Schmidt, A., Ceccopieri, W., Sartori, A., Franscoso, C., & Fontes, R. (2008). Is the meander growth in the Brazil Current system off Southeast Brazil due to baroclinic instability? *Dynamics of Atmosphere and Oceans*, *45*(3-4), 187–207. <https://doi.org/10.1016/j.dynatmoce.2008.01.002>
- Dee, D. P., Uppala, S. M., Simmons, A. J., Berrisford, P., Poli, P., Kobayashi, S., et al. (2011). The ERA-Interim reanalysis: Configuration and performance of the data assimilation system. *Quarterly Journal of Royal Meteorological Society*, *137*(656), 553–597. <https://doi.org/10.1002/qj.828>
- Deser, C., Alexander, M. A., & Timlin, M. S. (1999). Evidence for a wind-driven intensification of the Kuroshio Current Extension from the 1970s to the 1980s. *Journal of Climate*, *12*(6), 1697–1706. [https://doi.org/10.1175/1520-0442\(1999\)012<1697:EFAWDI>2.0.CO;2](https://doi.org/10.1175/1520-0442(1999)012<1697:EFAWDI>2.0.CO;2)
- Di Nezio, P. N., Gramer, L. J., Johns, W. E., Meinen, C. S., & Baringer, M. O. (2009). Observed interannual variability of the Florida Current: Wind forcing and the North Atlantic oscillation. *Journal of Physical Oceanography*, *39*(3), 721–736. <https://doi.org/10.1175/2008JPO4001.1>
- Dong, S., Baringer, M. O., Goni, G. J., Meinen, C. S., & Garzoli, S. L. (2014). Seasonal variations in the South Atlantic Meridional Overturning Circulation from observations and numerical models. *Geophysical Research Letters*, *41*, 4611–4618. <https://doi.org/10.1002/2014GL060428>
- Enfield, D. B., & Allen, J. S. (1980). On the structure and dynamics of monthly mean sea level anomalies along the Pacific Coast of North and South America. *Journal of Physical Oceanography*, *10*(4), 557–578. [https://doi.org/10.1175/1520-0485\(1980\)010<0557:OTSADO>2.0.CO;2](https://doi.org/10.1175/1520-0485(1980)010<0557:OTSADO>2.0.CO;2)
- Evans, D., & Signorini, S. (1985). Vertical structure of the Brazil Current. *Nature*, *315*(6014), 48–50. <https://doi.org/10.1038/315048a0>
- Evans, D. L., Signorini, S. R., & Miranda, L. B. (1983). A note on the transport of the Brazil Current. *Journal of Physical Oceanography*, *13*(9), 1732–1738. [https://doi.org/10.1175/1520-0485\(1983\)013<1732:ANOTTO>2.0.CO;2](https://doi.org/10.1175/1520-0485(1983)013<1732:ANOTTO>2.0.CO;2)
- Garzoli, S. L., & Garraffo, Z. (1989). Transports, frontal motions and eddies at the Brazil-Malvinas currents confluence. *Deep Sea Research Part A. Oceanographic Research Papers*, *36*(5), 681–703. [https://doi.org/10.1016/0198-0149\(89\)90145-3](https://doi.org/10.1016/0198-0149(89)90145-3)
- Gill, A. E., & Clarke, A. J. (1974). Wind-induced upwelling, coastal currents and sea-level changes. *Deep Sea Research*, *21*(5), 325–345. [https://doi.org/10.1016/0011-7471\(74\)90038-2](https://doi.org/10.1016/0011-7471(74)90038-2)
- Goes, M., Christophersen, J., Dong, S., Goni, G., & Baringer, M. O. (2018). An updated estimate of salinity for the Atlantic Ocean sector using temperature–salinity relationships. *Journal of Atmospheric and Oceanic Technology*, *35*(9), 1771–1784. <https://doi.org/10.1175/JTECH-D-18-0029.1>
- Goes, M., Goni, G., Hormann, V., & Perez, R. C. (2013). Variability of the Atlantic off-equatorial eastward currents during 1993–2010 using a synthetic method. *Journal of Geophysical Research: Oceans*, *118*, 3026–3045. <https://doi.org/10.1002/jgrc.20186>
- Goni, G., Kamholz, S., Garzoli, S., & Olson, D. (1996). Dynamics of the Brazil-Malvinas Confluence based on inverted echo sounders and altimetry. *Journal of Geophysical Research*, *101*(C7), 16,273–16,289. <https://doi.org/10.1029/96JC01146>
- Goni, G. J., Bringas, F., & DiNezio, P. N. (2011). Observed low frequency variability of the Brazil Current front. *Journal of Geophysical Research*, *116*, C10037. <https://doi.org/10.1029/2011JC007198>
- Gonzalez-Rodriguez, E., Valentin, J. L., Andre, D. L., & Jacob, S. A. (1992). Upwelling and downwelling at Cabo Frio (Brazil): comparison of biomass and primary production responses. *Journal of Plankton Research*, *14* (2), 289–306. <https://doi.org/10.1093/plankt/14.2.289>
- Häkkinen, S., Rhines, P. B., & Worthen, D. L. (2013). Northern North Atlantic sea surface height and ocean heat content variability. *Journal of Geophysical Research: Oceans*, *118*, 3670–3678. <https://doi.org/10.1002/jgrc.20268>
- Hautala, S. L., Roemmich, D., & Schmitz, W. J. Jr. (1994). Is the North Pacific in Sverdrup balance along 24°N? *Journal of Geophysical Research*, *99*(C8), 16,041–16,052. <https://doi.org/10.1029/94JC01084>
- Imawaki, S., Uchida, H., Ichikawa, H., Fukasawa, M., & Umatani, S. (2001). Satellite altimeter monitoring the Kuroshio Transport south of Japan. *Geophysical Research Letter*, *28*(1), 17–20. <https://doi.org/10.1029/2000GL011796>
- Laurindo, L. C., Mariano, A. J., & Lumpkin, R. (2017). An improved near-surface velocity climatology for the global ocean from drifter observations. *Deep-Sea Research Part I: Oceanographic Research Papers*, *124*, 73–92. <https://doi.org/10.1016/j.dsr.2017.04.009>
- Lima, M. O., Cirano, M., Mata, M. M., Goes, M., Goni, G., & Baringer, M. O. (2016). An assessment of the Brazil Current baroclinic structure and variability near 22°S in Distinct Ocean Forecasting and Analysis Systems. *Ocean Dynamics*, *66*(6-7), 893–916. <https://doi.org/10.1007/s10236-016-0959-6>
- Liu, Y., Liang, X. S., & Weisberg, R. H. (2007). Rectification of the bias in the wavelet power spectrum. *Journal of Atmospheric and Oceanic Technology*, *24*(12), 2093–2102. <https://doi.org/10.1175/2007JTECH0511.1>
- Lopez, H., Dong, S., Lee, S.-K., & Campos, E. (2016). Remote influence of interdecadal Pacific oscillation on the South Atlantic meridional overturning circulation variability. *Geophysical Research Letters*, *43*, 8250–8258. <https://doi.org/10.1002/2016GL069067>
- Majumder, S., Goes, M., Polito, P. S., Lumpkin, R., Schmid, C., & Lopez, H. (2019). Propagating modes of variability and their impact on the western boundary current in the South Atlantic. *Journal of Geophysical Research: Oceans*, *124*. <https://doi.org/10.1029/2018JC014812>
- Mémery, L., Arhan, M., Alvarez-Salgado, X. A., Messias, M. J., Mercier, H., Castro, C. G., & Rios, A. F. (2000). The water masses along the western boundary of the south and equatorial Atlantic. *Progress in Oceanography*, *47*(1), 69–98. [https://doi.org/10.1016/S0079-6611\(00\)00032-X](https://doi.org/10.1016/S0079-6611(00)00032-X)
- Mo, K. C., & Paegle, J. N. (2001). The Pacific-South American modes and their downstream effects. *International Journal of Climatology*, *21*, 1211–1229. <https://doi.org/10.1001/joc.685>
- Montgomery, R. B. (1941). Transport of the Florida Current off Habana. *Journal of Marine Research*, *4*(3), 198–219.
- Park, J., & Sweet, W. (2015). Accelerated sea level rise and Florida Current transport. *Ocean Sciences*, *11*(4), 607–615. <https://doi.org/10.5194/os-11-607-2015>
- Peterson, R. G., & Stramma, L. (1991). Upper-level circulation in the South Atlantic Ocean. *Progress in Oceanography*, *26*(1), 1–73. [https://doi.org/10.1016/0079-6611\(91\)90006-8](https://doi.org/10.1016/0079-6611(91)90006-8)
- Pezzi, L. P., Souza, R. B., Farias, P. C., Acevedo, O., & Miller, A. J. (2016). Air-sea interaction at the Southern Brazilian Continental Shelf: In situ observations. *Journal of Geophysical Research: Oceans*, *121*, 6671–6695. <https://doi.org/10.1002/2016JC011774>
- Pilo, G. S., Mata, M. M., & Azevedo, J. L. L. (2015). Eddy surface properties and propagation at Southern Hemisphere western boundary current systems. *Ocean Sciences*, *11*(4), 629–641. <https://doi.org/10.5194/os-11-629-2015>
- Piola, A. R., Romero, S. I., & Zajaczkovski, U. (2008). Space-time variability of the Plata plume inferred from ocean color. *Continental Shelf Research*, *28*(13), 1556–1567. <https://doi.org/10.1016/j.csr.2007.02.013>

- Polito, P. S., & Liu, W. T. (2003). Global characterization of Rossby waves at several spectral bands. *Journal of Geophysical Research*, 108(C1), 3018. <https://doi.org/10.1029/2000JC000607>
- Pontes, G. M., Sen Gupta, A., & Taschetto, A. S. (2016). Projected changes to South Atlantic boundary currents and confluence region in the CMIP5 models: The role of wind and deep ocean changes. *Environmental Research Letters*, 11(9), 094013. <https://doi.org/10.1088/1748-9326/11/9/094013>
- Reid, J. L., & Mantyla, A. W. (1976). The effect of the geostrophic flow upon coastal sea elevations in the northern North Pacific Ocean. *Journal of Geophysical Research*, 81(18), 3100–3110. <https://doi.org/10.1029/JC081i018p03100>
- Reynolds, R. W., Smith, T. M., Liu, C., Chelton, D. B., Casey, K. S., & Schlax, M. G. (2007). Daily high-resolution-blended analyses for sea surface temperature. *Journal of Climate*, 27(21), 8221–8228. <https://doi.org/10.1175/JCLI-D-14-00293.1>
- Ribeiro, F. N. D., Soares, J., & de Oliveira, A. P. (2011). A coupled numerical model to investigate the air–sea interaction at the coastal upwelling area of Cabo Frio, Brazil. *Environmental Fluid Mechanics*, 11(6), 551–572. <https://doi.org/10.1007/s10652-011-9220-5>
- Rocha, C. B., da Silveira, I. C. A., Castro, B. M., & Lima, J. A. M. (2014). Vertical structure, energetics, and dynamics of the Brazil Current System at 22°S–28°S. *Journal of Geophysical Research: Oceans*, 119, 52–69. <https://doi.org/10.1002/2013JC009143>
- Rodrigues, R. R., Campos, E. J., & Haarsma, R. (2015). The impact of ENSO on the South Atlantic subtropical dipole mode. *Journal of Climate*, 28(7), 269–2705.
- Rodrigues, R. R., Rothstein, L. M., & Wimbush, M. (2007). Seasonal variability of the South Equatorial Current Bifurcation in the Atlantic Ocean: A numerical study. *Journal of Physical Oceanography*, 37(1), 16–30. <https://doi.org/10.1175/JPO2983.1>
- Rodrigues, R. R., & Woollings, T. (2017). Impact of atmospheric blocking on South America in austral summer. *Journal of Climate*, 30(5), 1821–1837. <https://doi.org/10.1175/JCLI-D-16-0493.1>
- Schmid, C., & Majumder, S. (2018). Transport variability of the Brazil Current from observations and a data assimilation model. *Ocean Science*, 14(3), 417–436. <https://doi.org/10.5194/os-14-417-2018>
- Schmid, C., Schäfer, H., Zenk, W., & Podestá, G. (1995). The Vitória eddy and its relation to the Brazil Current. *Journal of Physical Oceanography*, 25(11), 2532–2546. [https://doi.org/10.1175/1520-0485\(1995\)025<2532:TVEAIR>2.0.CO;2](https://doi.org/10.1175/1520-0485(1995)025<2532:TVEAIR>2.0.CO;2)
- Soutelino, R. G., Silveira, I. C. A., Gangopadhyay, A., & Miranda, J. A. (2011). Is the Brazil Current eddy-dominated to the north of 20S? *Geophysical Research Letters*, 38, L03607. <https://doi.org/10.1029/2010GL046276>
- Stommel, H. (1965). *The Gulf Stream. A physical and dynamical description*, (2nd ed.p. 248). Berkeley: University of California Press.
- Thompson, K. R. (1986). North Atlantic sea-level and circulation. *Geophysical Journal International*, 87(1), 15–32. <https://doi.org/10.1111/j.1365-246X.1986.tb04543.x>
- Vianna, M. L., & Menezes, V. V. (2011). Double-celled subtropical gyre in the South Atlantic Ocean: Means, trends, and interannual changes. *Journal of Geophysical Research*, 116(C3), C03024. <https://doi.org/10.1029/2010JC006574>
- Waugh, D. W., Garfinkel, C. I., & Polvani, L. M. (2015). Drivers of the recent tropical expansion in the Southern Hemisphere: Changing SSTs or ozone depletion? *Journal of Climate*, 28(16), 6581–6586. <https://doi.org/10.1175/JCLI-D-15-0138.1>
- Wu, L., Cai, W., Zhang, L., Nakamura, H., Timmermann, A., Joyce, T., et al. (2012). Enhanced warming over the global subtropical western boundary currents. *Nature Climate Change*, 2(3), 161–166. <https://doi.org/10.1038/nclimate1353>
- Wunsch, C., Hansen, D. V., & Zetler, B. D. (1969). Fluctuations of the Florida Current inferred from sea level records. *Deep-Sea Research*, 16, 447–470.
- Wunsch, C., & Roemmich, D. (1985). Is the North Atlantic in Sverdrup Balance? *Journal of Physical Oceanography*, 15(12), 1876–1880. [https://doi.org/10.1175/1520-0485\(1985\)015<1876:ITNAIS>2.0.CO;2](https://doi.org/10.1175/1520-0485(1985)015<1876:ITNAIS>2.0.CO;2)
- Xue, Y., Reynolds, W., Banzon, V., Smith, T. M., & Rayner, N. A. (2011). [Global Oceans] Sea surface temperatures [in “State of the Climate in 2010”]. *Bulletin of American Meteorological Society*, 92(6), S78–S81.
- Yang, H., Lohmann, G., Wei, W., Dima, M., Ionita, M., & Liu, J. (2016). Intensification and poleward shift of subtropical western boundary currents in a warming climate. *Journal of Geophysical Research: Oceans*, 121, 4928–4945. <https://doi.org/10.1002/2015JC011513>
- Yu, P., Morey, S. L., & O'Brien, J. J. (2006). Development of new techniques for assimilating satellite altimetry data into ocean models. Available at: http://www.coaps.fsu.edu/~morey/GoM/08_Yu_Peng_WGNE_2006.pdf